

# Unveiling the superconducting scenario in multiphase superconductor CeRh<sub>2</sub>As<sub>2</sub> from space-group symmetry analysis and DFT calculations

V. G. Yarzhemsky,<sup>1,2</sup> E. A. Teplyakov,<sup>1,2</sup> S. V. Ereemeev,<sup>3,1</sup> and E. V. Chulkov<sup>4,1</sup>

<sup>1</sup>*Saint Petersburg State University, Saint Petersburg, Russia, 199034*

<sup>2</sup>*Kurnakov Institute of General and Inorganic Chemistry of RAS, 119071, Moscow, Russia*

<sup>3</sup>*Institute of Strength Physics and Materials Science of RAS, 634055 Tomsk, Russia*

<sup>4</sup>*Donostia International Physics Center, 20018 Donostia-San Sebastián, Spain*

(Dated: 2026/03/02)

Despite of the low transition temperature, the recently identified superconductor CeRh<sub>2</sub>As<sub>2</sub> has garnered significant interest due to its unique symmetry and magnetic characteristics, particularly the existence of two superconducting (SC) phases under a magnetic field, one of which exceeds the Pauli-Clogston limit. The field-induced transition from a low-field even-parity state to a high-field odd-parity state is usually described as a singlet-triplet transition. However, it is uncommon for a single compound to exhibit both triplet and singlet SC scenarios. The aim of this paper is to investigate the possibilities of symmetry changes in the SC state without a change of spin multiplicity. To this end, we construct the SC order parameter based on Anderson pair functions, considering the phase winding within the symmetry of the point group  $D_{4h}$  and the magnetic group  $4/mmm'$ . It was found that two triplets with opposite-spin and equal-spin pairing states of symmetry  $E'_{1u}$ , are nodeless but exhibit distinct internal structures and may be associated with low- and high-field phases. Additionally, nontrivial Cooper pairing resulting from the non-symmorphic structure of the space group was examined, particularly in the case where the Fermi surface intersects with the boundaries of a Brillouin zone (BZ). It was determined that at the X point, triplet pairs are even, while singlet pairs can be either even or odd. Furthermore, at the X point, pair density waves that alter phase by  $\pi$  at the atomic centers linked by lattice translations are also feasible. To explore the possibility of such scenarios, precise DFT calculations of the band structure were performed, revealing the contribution of Ce  $4f$  electrons to the states at the Fermi level. Thus, the even-odd transition can take place in a triplet scenario at symmetry points of a BZ.

## I. INTRODUCTION

In recently discovered superconductor CeRh<sub>2</sub>As<sub>2</sub>, the superconducting critical field of its high-field phase is as high as 14 T, although the transition temperature  $T_c$  is only 0.26 K [1]. Additionally, there is some instability in the state at  $T_0 = 0.4$  K. When the magnetic field is applied along the crystallographic  $c$  axis of the tetragonal cell, the superconducting state experiences a phase transition at  $H^* \sim 4$  T, which was identified by several thermodynamic probes [1]. The superconducting transition is completely suppressed down to 0.05 K at magnetic fields of 14 T for  $H||c$  and 2 T for  $H||ab$ . The upper critical field of the high-field phase denoted, as SC2, is not Pauli-Clogston-paramagnetically suppressed. In contrast, the low-field superconducting state (SC1) is strongly Pauli-Clogston-limited [1]. The phases SC1 and SC2 were interpreted as even and odd, respectively [1]. Remarkably, the SC phase-switching field  $H^*$  is drastically reduced under pressure, dropping to 0.3 T at 2.7 GPa [2]. It was suggested that the key superconducting properties of CeRh<sub>2</sub>As<sub>2</sub> are likely connected with the absence of local inversion symmetry in an overall inversion-symmetric crystal structure,  $P4/nmm$  (No. 129,  $D_{4h}^7$ ) [1].

The field-angle dependence of the upper critical field, as determined through magnetic  $ac$  susceptibility and specific heat measurements on single crystals of CeRh<sub>2</sub>As<sub>2</sub> has demonstrated the presence of odd-parity superconductivity in the SC2 phase, which is consistent

with the  $d$ -vector in the  $ab$  plane [3]. Note that  $d$ -vector in the  $ab$  plane corresponds to a triplet spin projection  $S_z = \pm 1$ , called equal spin pairing (ESP), and the  $d$ -vector normal to the plane corresponds to  $S_z = 0$ , called the opposite spin pairing (OSP) case [4]. Earlier DFT calculations indicated that the Fermi surface is primarily formed by the Ce  $4f$  electrons hybridizing with the Rh  $4d_{x^2-y^2}$  electrons, with the exception of the pockets near the A point [5]. Drawing from the similarities between experimental results and theoretical predictions [6], a pair density wave (PDW) scenario has been proposed for CeRh<sub>2</sub>As<sub>2</sub>.

In order to explain the existence of even and odd pairs in a single material, several models were proposed. The model in which the dominant interaction in pairs of electrons on the same sublattice is a spin singlet and the sublattices are swapped by space inversion  $I$ , resulting in the formation of even and odd-parity states, was suggested [7]. It has also been proposed that CeRh<sub>2</sub>As<sub>2</sub> hosts a quadrupole density wave (QDW) instability and the anomaly at  $T_0$  is a signature of the quadrupolar degrees of freedom [8]. The <sup>75</sup>As nuclear magnetic resonance (NMR) measurements revealed the presence of the antiferromagnetic (AFM) order within the SC1 phase and indicated that the AFM state disappears at the transition to the high-field SC2 phase [9]. Moreover, it was reported that the AFM order is inside the SC1 phase and that the AFM state disappears at the transition field to the high-field SC2 phase [10].

The transition between SC1 and SC2 in CeRh<sub>2</sub>As<sub>2</sub> was regarded as an even-odd parity within the  $C_{4h}$  symmetry and the superconducting order parameter (SOP) was expressed using linear combinations of spherical functions [11, 12]. Such a representation of the SOP resulted in the presence of solely point nodes of  $A_u$  in the  $k_z$  direction in  $C_{4h}$  symmetry [12].

Triplet pairing mechanisms derived from Hund's-Kondo model were also developed for CeRh<sub>2</sub>As<sub>2</sub> [13], and the role of non-symmorphic symmetry was pointed out. It is important to note that Hund's-like models assume one-center triplet correlations [14]. However, specific heat measurement outcomes characterize CeRh<sub>2</sub>As<sub>2</sub> as an antiferromagnetic superconductor, which undergoes a metamagnetic-like phase transition at  $T_0$  when subjected to magnetic fields applied along the  $c$  axis. This transition is associated with alterations in the spin structure and another change in the magnetic structure is observed at  $H \approx 4$  T. Neutron scattering experiments have identified AFM spin correlations, indicating that superconductivity in CeRh<sub>2</sub>As<sub>2</sub> is mediated by AFM spin fluctuations [15]. The muon spin relaxation ( $\mu$ SR) studies have demonstrated the coexistence of local magnetism and superconductivity [16]. Recent magnetic field-dependent measurements of magnetostriction and  $ac$  susceptibility confirmed the coexistence of the AFM phase that appears in the  $H||c$  field at  $T_0$  within both SC1 and SC2 phases [17]. The results of local magnetization measurements suggest fully-gapped superconductivity in the SC1 phase; however, the possibility of two-band superconductivity with a small  $d$ -wave gap function has not been ruled out [18].

Photoelectron spectroscopy measurements showed signs of Ce- $4f$  nesting on the Fermi surface at the X point [19]. Since at points on Brillouin zone (BZ) faces direct connection between multiplicity and parity of a Cooper pair may be violated [20] the pairing symmetry at this points may differ from that at generic points of a BZ. Therefore, in this work, special attention in the group-theoretical consideration and in the DFT calculations was given to such points.

A transition changing symmetry between two SC phases of CeRh<sub>2</sub>As<sub>2</sub> is typically regarded as a singlet-triplet transition. Nevertheless, the spin multiplicity determines the permutation symmetry, which in turn defines the sign of an exchange matrix element. Given the underlying magnetic structures, the possibility of Cooper pairing resulting from the exchange interaction between Ce  $4f$  electrons is considered the most likely scenario. Consequently, the presence of phases with different multiplicity would imply the presence of two different scenarios of superconductivity in a single material, which is unlikely.

The aim of this work is to study the possibility of changing the symmetry of Cooper pairs without changing the spin multiplicity of the pairs. It is worth noting that for a generic point in a BZ, the spatial part of a singlet (triplet) pair is even (odd) with respect to space

inversion, as demonstrated in both the phenomenological [21] and space-group [20] approaches. However, this direct relationship may be violated at BZ faces [20, 22, 23]. Earlier DFT calculations and photoelectron spectroscopy measurements have revealed multiple intersections of the Fermi surface (FS) with the BZ faces, attributed to the contributions of Ce  $4f$  electrons. Consequently, it can be inferred that the band structure of CeRh<sub>2</sub>As<sub>2</sub> is favorable to the appearance of Cooper pairs with unconventional symmetry.

In the present work SOP in phases SC1 and SC2 is considered making use of the space-group approach to the wavefunction of Cooper pair [20, 24]. This approach has previously yielded significant insights for non-symmorphic groups on the BZ faces [22, 23]. To support our findings, the DFT calculations for CeRh<sub>2</sub>As<sub>2</sub> were performed to confirm the Ce- $4f$  contribution at the intersections of FS with the BZ boundaries. Our analysis revealed intriguing relationships between the multiplicity and parity of the pair function at high-symmetry points M, X, and Z as well as on the boundary of BZ. Specifically, we identified possible symmetries of PDW at the X point. For the FS inside BZ the SOP was constructed on the basis of Anderson functions [25] incorporating phase winding for the point group  $D_{4h}$  and magnetic group  $4/mmm'm'$  [26, 27]. Additionally, we considered the spin-orbit coupling as direct products of spatial and spin parts of the Cooper pair wavefunction in point and magnetic group symmetry. Application of this technique revealed the possibility of a transition SC1  $\rightarrow$  SC2 with a change in the structure of the pair, but without altering its multiplicity, namely as an OSP  $\rightarrow$  ESP transition. To explore this possibility we constructed the SOP from functions of individual Cooper pairs, taking into account both spin-orbital coupling and phase winding [26, 27].

## II. METHODS

### A. Building of pair function and SOP

#### 1. Spatial part of pair function

In the present work we consider a single Cooper pair as a state of two equivalent electrons. According to Anderson's ansatz [25] the wavefunction of a Cooper pair is built from one-electron states taking into account the Pauli exclusion principle. Thus, for a generic point  $k$  in the BZ, the spatial parts of the wavefunctions for singlet and triplet pairs may be written by the following two relations, respectively:

$$\psi_k^s = \varphi_k(\xi_1)\varphi_{-k}(\xi_2) + \varphi_k(\xi_2)\varphi_{-k}(\xi_1) \quad (1)$$

$$\psi_k^t = \varphi_k(\xi_1)\varphi_{-k}(\xi_2) - \varphi_k(\xi_2)\varphi_{-k}(\xi_1) \quad (2)$$

It is clear from the above formulas that the functions  $\psi_k^s$  and  $\psi_k^t$  belong to IRs  $A_g$  and  $A_u$  of group  $C_i$ , respectively.

TABLE I. Possible symmetries of spatial parts of singlet and triplet pairs for the one-electron wavevector  $k$  at symmetry points, direction and planes in a BZ for space group  $P4/nmm$  ( $D_{4h}^7$ );  $t_i$  are projective representations [28].

$k$	IR( $H$ )	singlet pair	triplet pair	$d_\alpha$
planes				
(010), $k_y = 0$	all	$A_{1g} + B_{1g} + E_g$	$A_{2u} + B_{2u} + E_u$	$I$
(010), $k_y = \pi$	all	$A_{2g} + B_{2g} + E_g$	$A_{1u} + B_{1u} + E_u$	$I$
(001)	all	$A_{1g} + A_{2g} + B_{1g} + B_{2g}$	$2E_u$	$I$
(110)	all	$A_{1g} + B_{2g} + E_g$	$A_{2u} + B_{1u} + E_u$	$I$
lines				
$\Sigma$	all	$A_{1g} + B_{1g}$	$E_u$	$I$
$\Delta$	all	$A_{1g} + B_{2g}$	$E_u$	$I$
$\Lambda$	$A_i, B_i$	$A_{1g}$	$A_{2u}$	$I$
$\Lambda$	$E$	$A_{1g} + B_{1g} + B_{2g} + A_{1u}$	$A_{2u} + B_{1u} + B_{2u} + A_{2g}$	$I$
points				
$Z$	$A_i, B_i$	$A_{1g}$	–	$E$
$Z$	$E$	$A_{1g} + B_{1g} + B_{2g}$	$A_{2g}$	$E$
$M$	$t_1, t_2$	$A_{1g} + B_{2g} + B_{2u}$	$A_{1u}$	$E$
$M$	$t_3, t_4$	$A_{1g} + B_{2g} + A_{2u}$	$B_{1u}$	$E$
$X$	$t_1, t_2$	$A_{1g} + A_{2u} + B_{1g} + B_{2u} + E_u$	$E_g$	$E$
Pair density waves $K = (b_1/2, b_2/2, 0)$				
$X$	$t_1, t_2$	$t_2 + t_4(M)$	$t_1 + t_3(M)$	$\sigma_b$

The one-electron states in a crystal with a symmetry group  $G$  are defined by the wavevector  $k$ , its symmetry group  $H$  (little group) and the index  $\kappa$  of small IR  $D^\kappa$  of  $H$  [29]. A left coset decomposition of a space group  $G$  with respect to  $H$  is written as:

$$G = \sum_{\sigma} s_{\sigma} H. \quad (3)$$

The action of the representatives of the left cosets  $s_{\sigma}$  on the wave vector  $k$  results in a star  $\{k\}$  of the wave vector. An IR of the space group  $G$  is an induced representation  $D^\kappa \uparrow G$  defined by the following equation [29]:

$$(D^\kappa \uparrow G)_{\sigma i \rho j}(g) = \begin{cases} D_{ij}^{\kappa}(s_{\sigma}^{-1} g s_{\rho}), & \text{if } s_{\sigma}^{-1} g s_{\rho} \in H \\ 0, & \text{if } s_{\sigma}^{-1} g s_{\rho} \notin H \end{cases}, \quad (4)$$

where we use Bradley's notation an up arrow for induction [29].

The space group approach to the wavefunction of a Cooper pair [20] is based on the Anderson representation (1), (2) of a Cooper pair and on standard space-group representation theory for one-electron states (4). The methods to join these two statements are described elsewhere [20, 26, 27] and the details of the calculations are presented in Appendix. In the following, we briefly explain the physical background for the application of group theoretical methods.

It is seen in Eqs. (1) and (2) that in agreement with the Pauli exclusion principle the spatial part of a singlet (triplet) pair is symmetrical (antisymmetrical) with respect to the permutation of the electronic coordinates  $\xi_1$  and  $\xi_2$ . Thus, Anderson ansatz (1) may be generalized on the space groups by constructing symmetrized and antisymmetrized Kronecker squares  $D^\kappa \uparrow G \otimes D^\kappa \uparrow G$  of space group IRs (4). Bearing in mind the induced structure of space-group IRs one can use the Mackey-Bradley

theorem on symmetrized squares of induced representations [20, 30, 31]. The complete Kronecker square of dimension  $|\hat{G}|^2$  is decomposed into subsets corresponding to the decomposition of the space group into double cosets relative to the wavevector group:

$$G = \sum_{\delta} H d_{\delta} H. \quad (5)$$

Here and throughout  $\hat{G}$  stands for the central extension of the space group  $G$ , and the modulus sign denotes the number of elements in a group. The wavevector  $K_{\delta}$  of two-electron state, corresponding to the double coset  $d_{\delta}$  is defined by the relation:

$$k + d_{\delta} k = K_{\delta} + b, \quad (6)$$

where  $b$  is a reciprocal lattice vector.

The double coset defined by the inversion  $I$  corresponds to a Cooper pair:

$$k - k = 0. \quad (7)$$

For a double coset defined by an identity element  $E$  at the edges of a BZ, the following relation can also be fulfilled:

$$k + k = b, \quad (8)$$

In this case, two electrons with identical momenta are paired and the equality of the total momentum to zero is achieved due to the translational periodicity. If in Eq. (6)  $K_{\delta} = b_i/2$  the lattice translation  $T_i$  results in a phase factor  $\pi$  for the pair function and this case corresponds to PDW. Such case appears at point X, where  $X + X' = M$ . In a generic point of a BZ relation (7) holds and all even

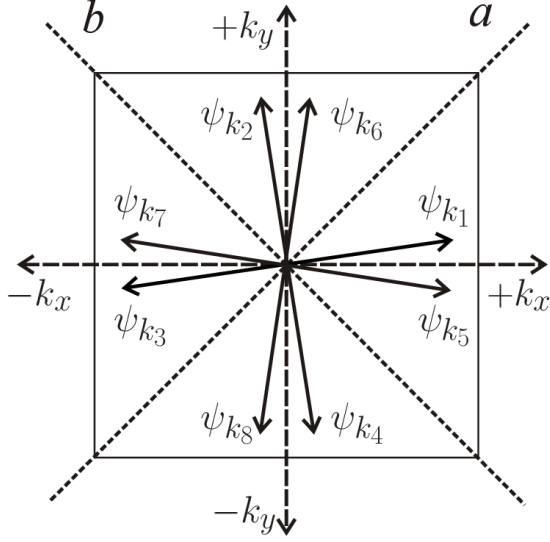


FIG. 1. Basis set of singlet and triplet pairs in  $D_{4h}$  group in a plane normal to  $k_z$  direction. The  $\psi_{k_i}$  denotes singlet or triplet pair function defined by Eq. (1). Subscript  $i$  corresponds to the action of the element of group  $C_{4v}$  on the initial vector  $k_1$ :  $k_2 = C_{4z}k_1$ ,  $k_3 = C_{2z}k_1$ ,  $k_4 = C_{4z}^3k_1$ ,  $k_5 = \sigma_y k_1$ ,  $k_6 = \sigma_a k_1$ ,  $k_7 = \sigma_x k_1$ ,  $k_8 = \sigma_b k_1$ .

(odd) IRs are permitted for singlet (triplet) pairs. but at symmetric points prohibitions on some IRs arise. The results of decomposition of Kronecker squares for symmetrical points in a BZ for group  $D_{4h}^7$  are presented in Table I. It is seen in Table I that at symmetry lines and planes some even (odd) IRs are forbidden. The intersection of such line (plane) with a FS results in point (line) node of Cooper pair wave function.

Anderson's Cooper pair wavefunctions (1) and (2) can be generalized on a space-group symmetry by making use of the standard projection operator technique for point groups, i.e. acting on a single pair function by all elements of point group [32]. For  $k$  in a generic point of a BZ the pair's symmetry is  $C_i$  and it is sufficient to use just elements of group  $C_{4v}$ . The basis set of a Cooper pair for  $k_1$  in the generic point of a BZ in  $D_{4h}$  symmetry is shown in Fig. 1. The basis is chosen in such a way that the action of elements of group  $C_{4v}$  results in permutations of elements  $\psi_{k_i}^{s(t)}$  without changing the sign. Also, singlet functions are invariant with respect to the inversion, while triplet functions change sign under the action of inversion. These reducible basis sets can be easily decomposed into irreducible sets belonging to IRs  $\Gamma^q$  of point group  $\hat{G}$  making use of standard projection operator technique for point groups [32]:

$$\Psi_i^{\Gamma^q} = \frac{|\Gamma^q|}{|\hat{G}'|} \sum_{h_j \in \hat{G}'} \Gamma_{ii}^q(h_j) h_j \psi_{k_1}^{s(t)}, \quad (9)$$

where  $\hat{G}' = C_{4v}$ .

When a vector  $k_1$  moves from the  $k_x$  axis in Fig. 1 to the  $a$  axis, all other basis functions pass through the

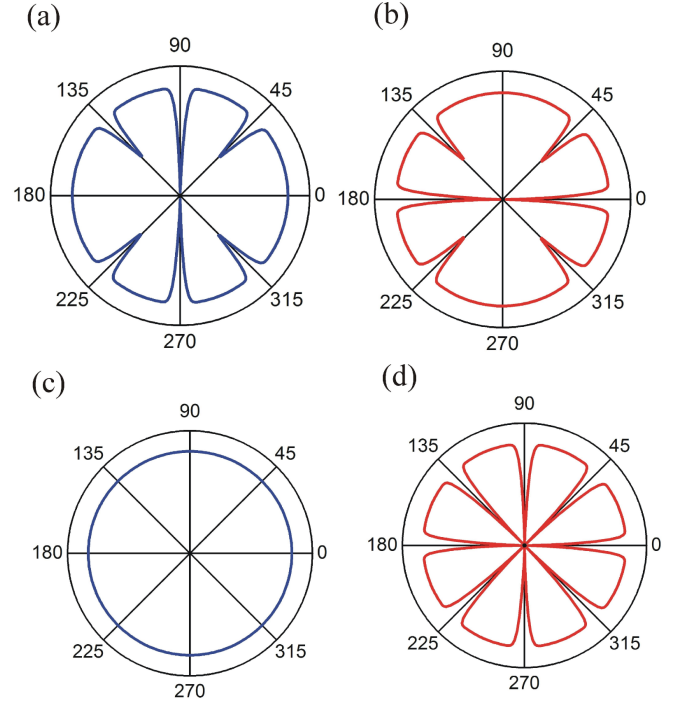


FIG. 2. Nodal structure of the SOP in a plane normal to  $k_z$  direction. (a)  $E_{g(u)}$  with  $m = 0$  and  $m = 1$ , (b)  $E_{g(u)}^{A_{2g}}$  with  $m = 0$  and  $m = 1$ , (c)  $E_{1g(u)}^{+}$  with  $m = 1$ ,  $E_{2g(u)}^{+}$  with  $m = -1$  and  $B_{g(u)}^{+}$  with  $m = 2$ , (d) the same as (c), but with  $-$  superscript. Note that the nodal structures with  $g$  and  $u$  subscripts differ in the basal plane (see Table I and the text).

entire circle. There is another free parameter - a phase winding  $\exp(im\theta)$  in the basis domain, where  $\theta$  is an angle between  $k_1$  and  $k_x$ . Rotational elements  $\theta_j$  of point group that translate a vector  $k_1$  into  $k_2$ ,  $k_3$  and  $k_4$  add additional phases:

$$\exp(im\theta_j) = \Gamma_{ii}^q(\theta_j). \quad (10)$$

Thus each one-dimensional IR and each two-dimensional IR, reduced to a diagonal form for rotations around a  $k_z$  axis, can be associated with a quasi-angular momentum  $\bar{m}$ . It is obvious that in order for the phase winding to be the same for all values of  $\theta$ , the quantities  $m$  and  $\bar{m}$  must be equated. In this way the SOP (total wavefunction of all pairs)  $\bar{\Psi}_{\Gamma^q}^{s(t)}$  in the plane normal to  $k_z$  direction is the superposition of wavefunctions of all pairs belonging to IR  $\Gamma^q$  of point group  $D_{4h}$ , and may be written as:

$$\bar{\Psi}_{\Gamma^q}^{s(t)}(\theta') = \sum_{\theta, h_j, i} \Gamma_{ii}^q(h_j) h_j \psi_k^{s(t)} \exp(im\theta), \quad 0 \leq \theta < \pi/4, h_j \in C_{4v}, \quad (11)$$

where  $\psi_k^{s(t)}$  is the initial function of type (1) or (2) with  $k$  taken near  $k_x$  axis ( $\theta = 0$ ). It is clear from the above discussion that  $\theta'$  runs in the interval from 0 to  $2\pi$ . In

this representation a single pair is characterized by quasi-angular momentum with respect to rotations of point group, but continuous phase winding of SOP is developed in pairs' condensate. Reflections interchange basis functions and add a phase factor  $-1$  in some cases, but do not affect a complex phase  $\exp(im\theta)$ . It is clear (see Fig. 1) that the directions of phase winding in adjacent sectors connected by reflection are opposite to each other and the total phase winding value equals to zero. It can be easily shown that in order to obtain a non-zero total phase winding, the mirror reflections of  $C_{4v}$  must be accompanied by complex conjugation (time reversal). This corresponds to magnetic group symmetry. Since inversion is already included in pair's symmetry, we come to the conclusion that the unitary subgroup of  $D_{4h}$  is  $C_{4h}$  and magnetic group is  $4/m\bar{m}'m'$ . Making use of Herring criterion (see e.g. Ref. [29]) we obtain that all ICRs (irreducible corepresentations) of  $4/m\bar{m}'m'$  belong to type (a), i.e. for unitary subgroup they are its IRs:

$$\Delta^\pm(R) = D(R), \quad R \in C_{4h}. \quad (12)$$

They are extended into the non-unitary left coset defined by  $A = \vartheta\sigma_y$  as:

$$\Delta^\pm(B) = \pm D(BA^{-1}), \quad B \in \vartheta C_{4h}. \quad (13)$$

The ICRs for group  $4/m\bar{m}'m'$  are given in Appendix. The ICRs are denoted in the present paper by IRs of unitary subgroup  $C_{4h}$  with the sign in superscript, corresponding to Eq. (13). It is clear that the value of quasi-angular momentum  $\bar{m}$  of ICR is the same as that of IR of the group  $C_{4h}$  defined by Eq. (10). Eqs. (9) and (11) can be generalized for magnetic groups by adding time-reversal  $\vartheta$  to operators  $h_j$  corresponding to non-unitary elements. Since the operator  $\vartheta$  is antilinear [29], reflections in vertical planes are accompanied with complex conjugation and the direction of the phase winding is the same in all sectors. In this case total phase winding is  $2\pi m$ . Since ICRs with  $+$  and  $-$  sign are possible, a phase difference on vertical plane may be zero or  $\pi$ . This means that, states with and without nodes are possible. In the present approach the SOP is constructed as a superposition of wavefunctions of all pairs, but its nodal structure is defined by the IR of a single pair. For example, when  $k_1$  in Fig. 1 approaches  $k_x$  axis the pair function  $\psi_{k_1}$  can cancel or merge with the pair function  $\psi_{k_5}$ . Which of the two cases is realized is determined by the sign of matrix element of IR  $\Gamma^q$  of point group in Eq. (9) for the reflection element. The plus and minus signs correspond to nodeless and nodal cases, respectively.

## 2. Spin part of pair function

In the axial symmetry triplet spin part  $(\hat{x}, \hat{y}, \hat{z})$  splits into the OSP (opposite spin pairing) part  $S_0^1 = \hat{z}$  and the ESP (equal spin pairing) part  $(\hat{x}, \hat{y})$ . For our purposes, it is more convenient to use complex linear combinations

that have certain values of projection of the angular momentum onto the  $z$  axis  $S_{\pm 1}^1 = \hat{x} \pm i\hat{y}$ . In the symmetry  $D_{4h}$  two components  $\hat{x} \pm i\hat{y}$  belong to the complex IR  $E_g$  and the  $\hat{z}$ -component belongs to IR  $A_{2g}$ . The characters of  $A_{2g}$  coincide with that of ICR  $A_g^-$  (see the appendix). This function is nodeless in the basal plane and has nodes in all vertical planes. Consider transformation properties of the  $\hat{x} + i\hat{y}$  component in the symmetry planes under the action of the elements of the point group:

$$\sigma_x(\hat{x} + i\hat{y}) = \hat{x} - i\hat{y}. \quad (14)$$

Hence, it follows that reflections change the spin projection. On the other hand, the reflection  $\sigma_x$  with time reversal does not change the spin projection:

$$\vartheta\sigma_x(\hat{x} + i\hat{y}) = \theta(\hat{x} - i\hat{y}) = \hat{x} + i\hat{y}. \quad (15)$$

Reflection  $\sigma_y$  with time reversal does not change the spin projection, but adds a phase factor  $-1$ :

$$\vartheta\sigma_y(\hat{x} + i\hat{y}) = \theta(-\hat{x} + i\hat{y}) = -\hat{x} - i\hat{y}. \quad (16)$$

Hence, it follows that the spin function  $\uparrow\uparrow = (\hat{x} + i\hat{y})$  belongs to the ICR  $E'_{1g}$  of the magnetic group  $4/m\bar{m}'m'$ . It can be shown by a similar way that the spin function  $\downarrow\downarrow = (\hat{x} - i\hat{y})$  belongs to ICR  $E'_{2g}$ . The action of the reflection in the basal plane changes the sign of the ESP spin function:

$$IC_{2z}(\hat{x} + i\hat{y}) = -\hat{x} - i\hat{y}, \quad (17)$$

which means that it is nodal in the basal plane.

## 3. Numerical calculation of SOP

In our approach SOP is a superposition of wavefunctions of all pairs. Since we are interested in the nodal structure in vertical planes, it is sufficient to consider the intersection of the FS with a plane perpendicular to the  $k_z$ -axis, which is approximated by a circle. In the case of phase winding with  $m = 1$  in  $D_{4h}$  symmetry, the phase difference between two sides of the vertical reflection plane may be complex. In this case, the structure of squared SOP may be obtained by computer modeling as follows. At 360 points on a circle, representing the intersection of FS with a plane normal to the  $k_z$  direction, the real and imaginary parts were modeled by Gaussians with a small half-width and complex coefficients corresponding to the theoretical phase. At each point, the sums of contributions of all pairs to the real and imaginary parts and the square of the modulus of this complex number were calculated. The square of the superposition of all pair's wavefunctions has the same physical meaning as the square of pair's function (which is identified with SOP) in the Ginzburg-Landau functional. The magnitude of the projection of the angular momentum  $m$  for the phase winding was chosen according to the Eq. (10), i.e.  $m = 1$  for IRs and ICRs of  $E-$  type and  $m = 2$  for IRs and ICRs of  $B-$  type. The results are presented in Fig. 2.

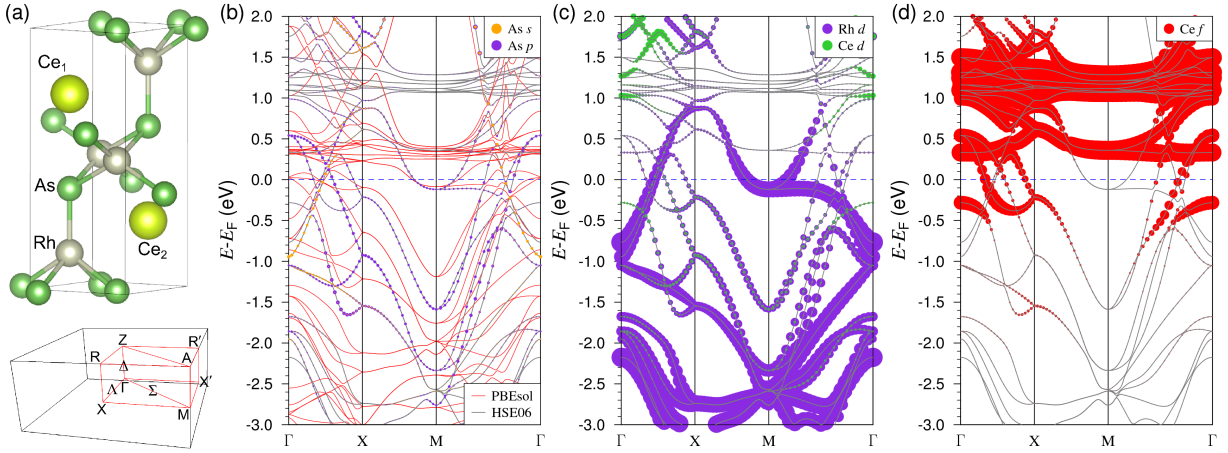


FIG. 3. (a) Tetragonal  $\text{CaBe}_2\text{Ge}_2$ -type atomic structure of  $\text{CeRh}_2\text{As}_2$  (top) and corresponding bulk Brillouin zone (bottom) with indication of the high-symmetry points and high-symmetry directions. The bulk electronic band structure of  $\text{CeRh}_2\text{As}_2$  calculated with the GGA-PBESol and the HSE06 hybrid functional with weights of the As- $s, p$  (b), Rh(Ce)- $d$  (c), and Ce- $f$  (d) orbitals.

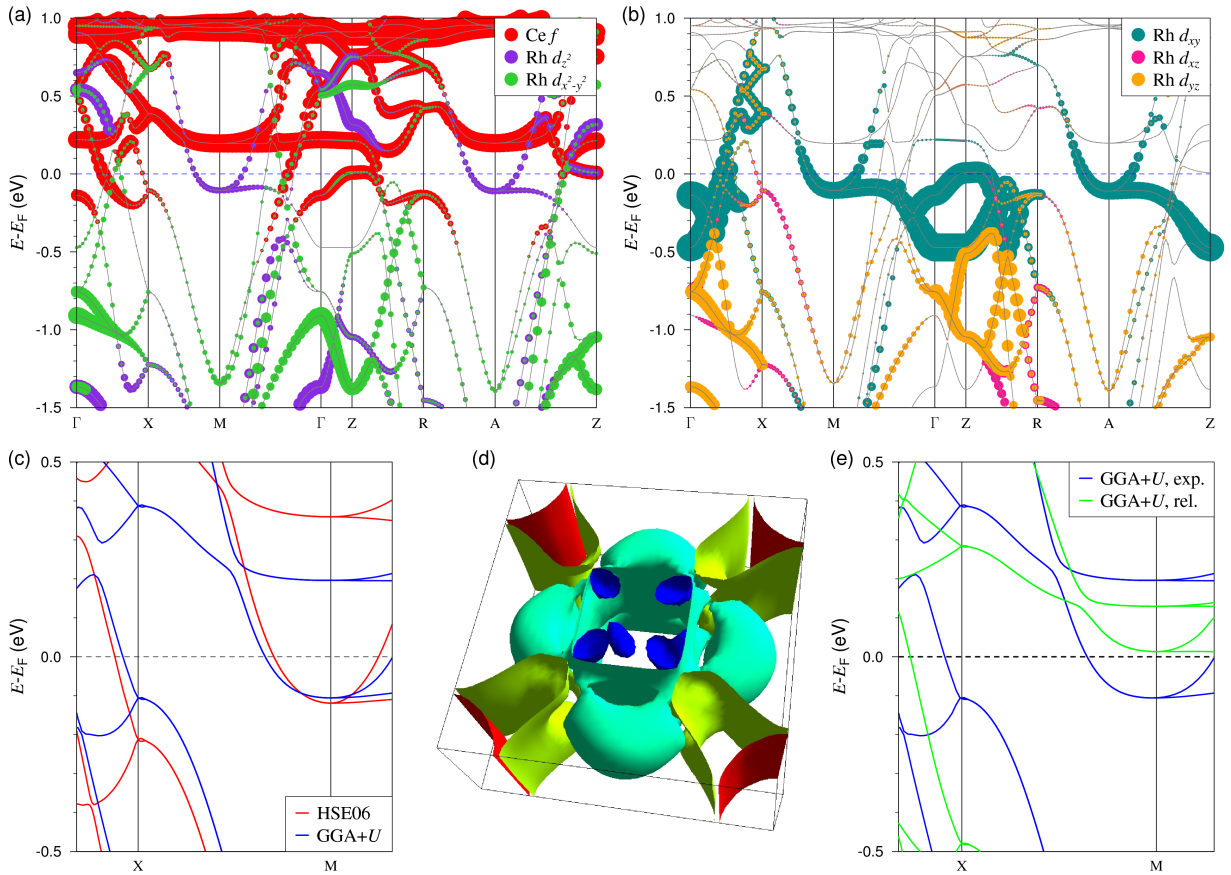


FIG. 4. Bulk electronic band structure calculated within GGA+ $U$ : (a) Ce- $f$  and Rh- $e_g$ ; (b) Rh- $t_{2g}$  orbitals. (c) Magnified view of the GGA+ $U$  band structure in the vicinity of X and M points in comparison with HSE06 result. (d) Calculated Fermi surface. (e) Comparison of low-energy spectra calculated with experimental and relaxed atomic structure parameters.

## B. DFT calculations

Electronic structure calculations were carried out within the density functional theory using the projector augmented wave (PAW) method [33] as implemented in the VASP code [34, 35]. To obtain accurate bulk band structure, the HSE06 screened hybrid functional [36] was adopted. Since hybrid functional approach is resource consuming for Fermi surface calculations the correlation effects were included within the GGA+ $U$  method [37]. The values of the screened Coulomb  $U$  and Hund  $J$  interaction parameters for Ce  $4f$  electrons were obtained variationally to fit the  $4f$  bands position calculated with HSE06. The Fermi surface was determined on a dense  $24 \times 24 \times 10$   $k$ -point mesh and visualized by using FermiSurfer [38].

## III. RESULTS

### 1. Electronic structure

Previous DFT calculations [5, 12] resulted in some intersections of FS with faces of a BZ. The pairing of electrons with  $k$  vectors on the faces of a BZ can violate the direct connections between multiplicity and parity of a pair that follow from the Anderson ansatz (1), (2) in generic  $k$ -points [20]. In order to estimate the contribution of Ce  $4f$  electrons in symmetry points of a BZ, new more sophisticated DFT calculations were carried out in the present work.

We begin with a standard DFT with the PBEsol exchange-correlation functional [39]. As a starting point, we use experimental crystal structure parameters (both lattice constants and atomic positions, Fig. 3(a) adopted from Ref. [1]. The resulting bulk band structure (Fig. 3(b), red lines) partially reproduces earlier calculations [5, 19, 40, 41] were performed without and with the Ce- $4f$  correlations. The latter was incorporated within the GGA+ $U$  with a relatively small Hubbard parameter ( $U = 2$  eV). Across all calculations, including ours, the position of the Ce- $4f$  band was found to be slightly above the  $E_F$ . The difference from earlier calculations is the appearance of an electron band intersecting the  $E_F$  at the M point, which was unoccupied in previous works. In the following, we will show that this difference is related to lattice relaxation, which we do not include yet here.

The spectrum calculated with the screened hybrid functional HSE06, which more accurately depicts the correlation effects, shows that the position of the dispersionless unoccupied  $f$ -band is much higher, above +1 eV (Fig. 3(b), gray lines). The change in the position of the  $f$  band does not affect the M point band while it essentially modifies the dispersions of the states along the  $\Gamma - X$  and  $\Gamma - M$  directions near the Fermi level. This distinction in the effect of the  $f$  band position on the states at the Fermi level is rooted in their distinct orbital

compositions. The electronic state at the M point is completely composed of the  $d$  electrons of rhodium (Fig. 3(c)) whereas the  $\Gamma$ -centered hole-like states involve a significant  $f$  contribution (Fig. 3(d)). Note that the contribution of arsenic orbitals to the states near  $E_F$  is negligibly small (Fig. 3(b)). This analysis underscores the importance of employing advanced functionals such as HSE06 for precise predictions of electronic structure, particularly when subtle orbital effects influence material properties.

Next we turn to a simplified approach, namely GGA+ $U$ , adjusting the Hubbard  $U$ , and Hund  $J$  interaction parameters for cerium  $f$  orbitals to match the position of the  $f$  band obtained with the HSE06 functional. We found that at  $U$  up to 5 eV the position of the  $f$  band remains almost unchanged, approximately at +0.5 eV, similar to the GGA calculation. Only with Hubbard  $U = 10$  eV the position of the  $f$  band reaches +1 eV (Fig. 4(a)). This also requires a rather large parameter  $J$ , 2 eV, because there are convergence problems with smaller values. Overall, the obtained GGA+ $U$  band spectrum agrees well with the HSE06 result. Figs. 4 (a,b) show the detailed symmetry of Rh  $d$  states along high-symmetry directions in the bulk Brillouin zone. In particular, the M band, which also persists at  $k_z = 0.5$  (the A point), is primarily composed of Rh  $d_{xy}$  orbitals with a minor  $d_{z^2}$  contribution. It should be noted that the M band is well resolved in ARPES [41]. Its energy and dispersion are described within GGA+ $U$  with an accuracy of HSE06 (Fig. 4(c)) and since it does not exhibit a  $k_z$  dependence it leads to the formation of cylindrical sheets of the Fermi surface, centered at the corners of the Brillouin zone (Fig. 4(d)).

The next state we will focus on is the band at the X point, which is also observed in ARPES and its analysis has been the subject of previous papers [19, 41]. High-resolution ARPES measurements revealed a band with an electron-like dispersion along  $\Gamma - X - \Gamma$  and a hole-like dispersion along the  $M - X - M$  direction, indicating the existence of a van Hove singularity (VHS) at the X point. The binding energy of the VHS was found to be approximately  $75 \pm 60$  meV [41]. Notably, our GGA+ $U$  calculations place the X-band  $\approx 100$  meV below  $E_F$ , agreeing well with experiment, unlike HSE06 calculations, in which the VHS lies a hundred meV lower (Fig. 4(c)).

Finally, we examined the effect of structural relaxation on the low-energy bulk spectrum. We found that the relaxation only subtly altered the lattice parameters of CeRh<sub>2</sub>As<sub>2</sub>, contracting them by roughly  $\approx 1$  %, specifically  $a = b$  by 0.91 % and  $c$  by 1.04 %, compared to their experimental values [1]. However, it significantly modifies interlayer distances within the cell: the relaxed Rh-As interlayer distances within Rh-As-Rh and As-Rh-As trilayers shortened by 12.7 % and expanded by 14.8 %, respectively, relative to the interlayer distances, derived from the accurate experimentally measured atomic coordinates [1]. Along with this, Ce-Rh and Ce-As interlayer distances also undergo significant relaxation dis-

placements, by +6.9 % and -10.5 %, respectively. These substantial atomic structural changes, despite negligible changes in the lattice parameters, strongly modify the band structure (Fig. 4(e)). The occupied band at the M point becomes depleted, consistent with prior calculations [5, 19, 40, 41], where the lattice relaxation was also taken into account. At the same time, the VHS state at the X point after relaxation lies much lower, approximately at 0.5 eV below  $E_F$ , contradicting ARPES results ( $75 \pm 60$  meV [41]). Therefore, DFT relaxation appears to induce unrealistically large internal atomic distortions and the electronic band spectrum of such a relaxed structure contradicts experimental observations.

## 2. Spatial part of pair function inside the BZ and on its faces

Possible IRs for singlet and triplet pair functions on symmetry points, lines, and planes in a BZ obtained by the Mackey-Bradley theorem are presented in Table I. The absence of any IR on a symmetry line or plane means group-theoretical point or line node of the pair function belonging to this IR. When comparing the data of Table I with the characters of IRs of  $D_{4h}$  presented in the Appendix we see that the negative characters of the one-dimensional IRs in all planes and of two-dimensional IR in basal plane correspond to nodal planes. Characters of  $E_{g(u)}$  in vertical planes equal to zero and nodes depend on the unitary transformation. These nodes and dips will be considered later by numerical calculations. Due to the non-symmorphic structure of the space group, nontrivial pairing symmetry appears on the faces of a BZ. On the faces of a BZ normal to  $k_y$  (plane X'MAR', see Fig. 3 (a, bottom)) singlet  $A_{1g}$  pairs are forbidden. At points M and X, singlet odd pairs are possible, and at points X and Z, triplet pairs are even. Also, at point X, coupling of two electrons with  $k = b_1/2$  and  $k = b_2/2$  results in PDW pairs with  $K = (b_1/2, b_2/2, 0)$ . In this case, a gap function changes the sign under the action of single lattice translations  $t_1$  or  $t_2$ .

Now let us move on to the consideration of two-dimensional IRs at generic points of a BZ, where all even (odd) IRs are possible for singlet (triplet) pairs. It is immediately verified that a multiplication of  $E_{g(u)}$  by  $A_{2g}$  results in also IR  $E_{g(u)}$ , which we denote by the superscript  $A_{2g}$ . Since the characters of  $A_{2g}$  equal to -1 for reflections in vertical planes, this transformation reverses the nodal structure in vertical planes. Inside the sectors, the interference is almost constructive and the squared SOP is constant. Interference of pair's functions located on both sides of the symmetry plane can lead to the appearance of nodes and dips of the squared SOP. The matrices of  $\tilde{E}_g$  and  $\tilde{E}_u$  in diagonal complex form for rotations  $C_4$  are presented in the Appendix. Since the matrices of  $\tilde{E}_g$  and  $\tilde{E}_u$  are chosen in such a way that they coincide on the subgroup  $C_{4v}$ , the nodal structures of SOP in vertical planes in Figs. 2 (a) and (b) are the

same for  $\tilde{E}_g$  and  $\tilde{E}_u$ . The structure in Fig. 2 (b) corresponds to the multiplication of the IR  $\tilde{E}_g$  or  $\tilde{E}_u$  by  $A_{2g}$ . Computer calculations showed that the structures without phase winding and with phase winding with  $m = \pm 1$  are the same. Both structures in Figs. 2 (a) and (b) are characterized by dips in both diagonal planes. Structure in Fig. 2 (a) is nodeless, but the structure corresponding to IR  $\tilde{E}_g$  multiplied by  $A_{2g}$  has nodes in planes normal to the axes  $k_x$  and  $k_y$ . Thus, the nodes of  $\tilde{E}_g$  and  $\tilde{E}_u$  in vertical planes are topological, i.e., they can be removed by a unitary transformation that does not change the characters. Nodes in the basal plane do not depend on unitary transformations and they are the same as those obtained using the Mackey-Bradley theorem (see Table I), namely  $\tilde{E}_g$  is nodal and  $\tilde{E}_u$  is nodeless in the basal plane. Calculations showed that nodes of one-dimensional IRs  $B_{1(2)g(u)}$  in the chiral case are the same as those that follow from group theory (see Table I) and they are not shown in Fig. 2. Since in the chiral case, the phase winding directions in the sectors connected with reflections are opposite, total phase winding is zero. Basis functions of ICRs can be easily constructed using Eq. (9) by replacing  $h_j$  with  $h_j\vartheta$  for anti-unitary elements. Thus, we can write the expression for the ICR originating from the IRs  $E'_{1g(u)}^\pm$  of  $C_{4h}$ :

$$\Psi \left( E'_{1g(u)}^\pm \right) = (\psi_{k_1}^{s(t)} + i\psi_{k_2}^{s(t)} - \psi_{k_3}^{s(t)} - i\psi_{k_4}^{s(t)})e^{i\theta} \pm (\psi_{k_5}^{s(t)} - i\psi_{k_6}^{s(t)} - \psi_{k_7}^{s(t)} + i\psi_{k_8}^{s(t)})e^{-i\theta}. \quad (18)$$

Note that since reflections change the direction of the contour traversal, the phase winding direction is the same in all sectors. For example, the element  $\vartheta\sigma_y$  transforms the two points  $\theta = 0$  and  $\theta = \pi/4$  with phases  $\phi = 0$  and  $\phi = \pi/4$  into the points  $\theta = 0$  and  $\theta = -\pi/4$  with phases  $\phi = 0$  and  $\phi = -\pi/4$  and the phase winding direction remains unchanged.

In magnetic group symmetry, the nodal structures of SOP in vertical planes are the same for all ICRs with a plus sign and for all ICRs with a minus sign (see Figs. 2 (c) and (d), respectively). Note that in numerical calculations  $m = 1$  for  $E'_{g(u)}^\pm$  and  $m = 2$  for  $B'_{g(u)}^\pm$  were used. However, in the magnetic symmetry  $4/mmm'm'$  the total phase winding is  $2\pi m$  in both nodeless and nodal cases. In the case of the magnetic group  $4/mmm'm'$  with phase winding  $m = 1$  for  $E'_{1g(u)}^+$  and  $m = 2$  for  $B'_{g(u)}^+$ , the resultant SOPs have no nodes in vertical planes, but SOPs  $E'_{1g(u)}^-$  and  $B'_{g(u)}^-$  have nodes in all vertical planes, as shown in Figs. 2 (c) and (d), respectively.

Thus, we have obtained that with axial symmetry, the nodes on vertical symmetry planes can be removed in magnetic symmetry with phase winding, if the phase winding parameter  $m$  corresponds to the character of the IR (see Eq. (10)). At the same time, the nodes on the basal plane are uniquely related to the projection of the angular momentum and are robust. Indeed, for  $C_{2z}$  rotation characters equal to -1 and +1 for  $m = 1$  and  $m = 2$ , respectively. Since reflection in the basal plane

equals to  $IC_{2z}$ , we obtain for  $m = 1$  that  $\chi_g(\sigma_z) = -1$  and  $\chi_u(\sigma_z) = +1$  for even and odd pairs, respectively. Similarly, at  $m = 2$ , we obtain that  $\chi_g(\sigma_z) = 1$  and  $\chi_u(\sigma_z) = -1$ . Thus, robust nodes in the basal plane appear at  $m = 1$  and for even pairs and at  $m = 2$  for odd pairs. And vice versa: even pairs with  $m = 2$  and odd pairs with  $m = 1$  are nodeless in basal plane.

### 3. Total pair function inside the BZ

It follows from the above discussion that in a singlet case there are two nodeless states, corresponding to experimental data for the SC1 phase [18], namely ICR  $B_g^+$  with phase winding  $m = 2$  in the magnetic group  $4/mmm'$  symmetry and IR  $A_{1g}$  without phase winding in  $D_{4h}$  symmetry.

In a triplet case nodeless spatial part in  $4/mmm'$  symmetry belongs to ICR  $E_{1u}^+$  with phase winding  $m = 1$ . The total pair function is a direct product of its spatial and spin parts. In axial symmetry, the triplet spin function splits into ESP and OSP parts belonging to  $E_{1g}^-$  ( $E_{2g}^+$ ) and  $A_g^-$  respectively. Multiplying the nodeless spatial part of a triplet pair  $E_{1u}^+$  by  $A_g^-$  results in nodal  $E_{1u}^-$ . Although when multiplying the  $E_{1u}^-$  spatial part by the spin part  $A_g^-$  we obtain the nodeless total pair function  $E_{1u}^+$ . In  $D_{4h}$  symmetry, multiplication of the ESP spin part  $\tilde{E}_g$  (nodal in the basal plane) by the triplet spatial part  $\tilde{E}_u$  (nodeless in the basal plane) results in IRs  $A_{1u} + A_{2u} + B_{1u} + B_{2u}$ , which are nodal in the basal plane. This coupling of spatial and spin parts of a Cooper pair is similar to angular momentum coupling in atomic physics. Indeed two lines of two-dimensional IRs correspond to angular momentum projections  $+1$  and  $-1$  and in the direct product there are terms  $m = 2$ ,  $m = -2$ , and two terms with  $m = 0$ , which correspond to  $B_{1u}$ ,  $B_{2u}$ ,  $A_{1u}$  and  $A_{2u}$ .

Similar angular momentum coupling takes place in  $4/mmm'$  symmetry. When multiplying the ESP function  $E_{1g}^-$  by the spatial part  $E_{1u}^-$  or  $E_{2u}^-$ , we obtain  $B_u^+$  or  $A_u^+$ , respectively. There is some similarity and some difference between our results and the results of the order parameter modeling with spherical functions [11]. Our functions  $E_{1u}^+$  or  $E_{2u}^+$  are similar to functions  $E'_u$  and  $E''_u$  [11]; however, our helical functions  $B_u^+$  may have angular momentum projection  $m = 2$  and phase winding  $4\pi m$ , but the angular momentum of  $B_u$  is not expressed explicitly [11]. The model approach [11] resulted in a fully gapped  $A_u$  in  $C_{4h}$  symmetry. In the present space-group approach, the IR  $A_{1u}$  of the  $D_{4h}$  group has nodes in all planes (see Table I). The nodes in vertical planes of  $A_{1u}$  may be removed by consideration of  $A_u^+$  with the phase winding  $m = 4$ , but, as was shown above, nodes on the basal plane of an odd function with  $m = 4$  are robust. Recent results of local magnetization measurements indicated fully-gapped superconductivity [18] in the SC1 phase and staggered magnetization in the basal

plane. This may correspond to singlet  $A_{1g}$  pairs. We obtained that there are two additional options for fully gapped triplet functions both of symmetry  $E_{1u}^+$ . This ESP state is consistent with a  $d$ -vector in the  $ab$ -plane [3]. The OSP case corresponds to the triplet spatial part  $E_{1u}^-$  with  $m = 1$ , and in the ESP case to the triplet spatial part  $B_u^-$  with  $m = 2$ . Note that despite the same full symmetry  $E_{1u}^+$  and total angular momentum, the structure of these pairs is different. In the OSP pair, the electron spin projections are opposite and the angular momentum is determined by the spatial part. In this case, the magnetic field leads to the destruction of pairs. In the ESP case, the angular momentum can be determined only by the spin or by the sum of the angular momentum of the spin and spatial part. In this case, the magnetic field does not destroy the pair, but rather maintains the electron spins in one direction. Also, a singlet  $A_{1g}$  is nodeless and can't be ruled out for a low-field state.

## IV. DISCUSSION

The above considered group theoretical results may be used to build models of parity changing transition without changing of pairing potential. It is very remarkable that the crystal structures of the heavy fermion superconductors containing  $d$  and  $f$  electrons, e.g., UPt<sub>3</sub>, UBe<sub>13</sub>, LiPt<sub>3</sub>B, and also of recently discovered UTe<sub>2</sub> and CeRh<sub>2</sub>As<sub>2</sub>, are non-symmorphic [22]. Below, we will shed light on the relationship between superconductivity and non-symmorphic structure within the framework of the nearest-neighbor exchange interaction model.

There are two nonequivalent Ce atoms per unit cell, denoted as Ce<sub>1</sub> and Ce<sub>2</sub> (see Fig. 3(a)), and there is no inversion symmetry at either Ce atom. However, the two nonequivalent Ce atoms are inversion symmetry partners of each other, so there is global inversion symmetry. For  $k$  being a generic point in the BZ, the IR of the space group  $D_{4h}^7$  is defined by a 16-dimensional wavevector star (see Eq. (4)). Half of the wavevector star is shown in Fig. 1. This set of prongs, which we call upper set, is invariant with respect to the point group  $C_{4v}$ , and another half of the prongs (lower set, which is not shown in Fig. 1) is obtained by the action of the element  $\{I|\tau\}$ . Improper translation  $\tau$  is not essential for the construction of IRs of the space group inside the BZ, but it is important for construction of the basis set.

The basis set belonging to an IR of a space group may be constructed from atomic states, making use of projection operators (see Eq. (9)), where the sum runs over all point group elements and all lattice translations  $T$ . The action of the elements of  $C_{4v}$  on the initial  $k$  vector results in the prongs of the upper set shown in Fig. 1. Since the local subgroup of Ce<sub>1</sub>  $4f$  functions is  $C_{4v}$ , they are projected on the  $k$  vectors of the upper set. Since the translation subgroup  $T$  belongs to the wave vector group, the basis functions of all sublattice  $Ce_1 \times T$  are projected

on the prongs of the upper face. The elements of the left coset  $\{I|\tau\}C_{4v}$  interchange sublattices and also the prongs connected by space inversion. Due to exchange interaction between nearest neighbors the lowest energy will correspond to the triplet term of electrons on two Ce atoms with antisymmetrized spatial part. According to the group theory, the scalar interaction is possible between the states belonging to the same row of the same IR only. As we demonstrated above the wavefunctions of two Ce atoms connected by  $\{I|\tau\}$  belong to opposite  $k$  vectors, i.e. different rows of IR, and hence, the exchange interaction between them is symmetry forbidden. In a Cooper pair the opposite  $k$  vectors cancel each other ( $K_\delta = 0$ ) and hence the exchange interaction between nearest neighbors is not restricted by the symmetry. On the other hand, in symmorphic groups equivalent atoms are connected by translations belonging to  $T$ . Since  $T$  belongs to the wavevector group in all cases, the atomic functions of nearest neighbors belong to the same  $k$  vector, i.e. to the same row of IR and hence, the exchange interaction between them is possible without Cooper pairing. Thus, the exchange interaction of electrons on two nearest neighbors atoms connected by  $\{I|\tau\}$  can cause Cooper pairing in non-symmorphic space groups only.

To acquire the parameter of the model, we evaluated the exchange integral for  $4f$  electrons on Ce<sub>1</sub> and Ce<sub>2</sub> atoms located at an interatomic distance of 5.7 Å, using Ce Hartree-Fock atomic functions, and determined that the exchange integral  $G(4f_1, 4f_2)$  equals  $2.7 \times 10^{-5}$  eV. This value corresponds to the order of magnitude of  $T_c$  of CeRh<sub>2</sub>As<sub>2</sub> [1]. Hence, it follows that our model of Cooper pairing due to exchange interaction between two Ce atoms connected by the element  $\{I|\tau\}$  is energetically possible.

Earlier the spin-singlet AFM superconductivity was proposed on the base of the NMR measurements [10]. However, it should be noted that, strictly speaking, NMR may distinguish between even and odd spatial functions and this result may correspond to OSP triplet pairs at the X point, which are even (see Table I). According to our DFT calculations (Fig. 3(d)), the bands with a large contribution of Ce- $4f$  electrons, intersects the Fermi level in the  $\Gamma - X$  direction near the X point. Thus, the SC1 state can be explained in terms of even triplet OSP pairing at X. Antiferromagnetism is no longer observed upon the parity transition to the high-field SC2 state [10]. Within our model this behavior can be connected to odd ESP triplet pairs in the  $\Gamma - X$  direction.

Thus, the proposed scenario, based on space group symmetry, and DFT calculations can explain the symmetry changing transition in CeRh<sub>2</sub>As<sub>2</sub> within a single pairing potential, namely nearest-neighbor exchange interaction of Ce- $4f$  electrons. Our findings also allow us to propose a parity-change scenario for singlet pairs. Indeed, our DFT and ARPES [19] results have shown the presence of the Fermi surface pockets centered at the M

point (Fig. 4(d)), which are populated by Rh- $4d$  orbitals (Fig. 4(a,b)). The VHS state at X below  $E_F$  is contributed both Ce- $4f$  and Rh- $4d$  orbitals. Given the non-symmorphic structure of the space group, singlet pairs at the X and M points can be either even or odd (see Table I). Consequently, it follows that the even-odd transition can be described as, for example, an  $A_{1g} \rightarrow B_{2u}$  transition of singlet pairs at symmetry points on the faces of a BZ.

Very recently, it has been discovered that the superconductor LaRh<sub>2</sub>As<sub>2</sub>, which shares the same crystal structure as CeRh<sub>2</sub>As<sub>2</sub> and has a similar critical temperature ( $\approx 0.3$  K), exhibits conventional full-gap  $s$ -wave type-II superconductivity. This is characterized by a small upper critical field  $H_{c2}$  of about 10 mT (see Ref. [42]). In this forthcoming paper, comparing LaRh<sub>2</sub>As<sub>2</sub> and CeRh<sub>2</sub>As<sub>2</sub>, the authors suggest that the  $4f$  electrons in the latter case not only enhance the orbital limiting field but also play a role in the development of unconventional superconductivity with SC multiphase. Therefore, it can be concluded that our first scenario, which is based on the exchange interaction between the  $4f$  electrons of the nearest neighbor Ce atoms, is more realistic.

## V. CONCLUSION

The SOP symmetries of CeRh<sub>2</sub>As<sub>2</sub> were scrutinized on the basis of Anderson functions for single pairs with taking into account phase winding, time-reversal symmetry and the non-symmorphic structure of the space group. It has been established that the non-symmorphic structure of the space group of CeRh<sub>2</sub>As<sub>2</sub> disrupts the direct relationship between the multiplicity and parity of Cooper pairs at the high-symmetry points of the Brillouin zone. This finding make possible to explain different spatial parities of two superconducting phases within a single pairing interaction. It was obtained that in axial symmetry the nodes in vertical planes may be removed by phase winding in the magnetic group symmetry  $4/m\bar{m}'m'$ , but the nodes in the basal plane are unremovable. The spin-orbit coupling was considered in magnetic symmetry, and it was obtained that nodeless SOP belongs to ICR  $E'_{1u}^+$  at generic point of the Brillouin zone in ESP and OSP triplet cases. At the OSP  $\rightarrow$  ESP transition, an external magnetic field should destroy OSP pairs and stabilizes ESP pairs. It was also obtained that triplet pairs at the X point are even. Thus, the SC1 and SC2 phases may be connected with even triplet ESP pairs at the X point and odd triplet ESP pairs in the  $\Gamma - X$  direction, respectively. In this scenario spatial parity changes without a changing of the parity with respect to permutation of electronic coordinates and, consequently, without a changing of the sign of the exchange integral between  $4f$  orbitals of two non-equivalent Ce atoms. This finding highlights the complexities involved in understanding the behavior of Cooper pairs in non-symmorphic systems.

- [1] S. Khim, J. F. Landaeta, J. Banda, N. Bannor, M. Brando, P. M. R. Brydon, D. Hafner, R. K uchler, R. Cardoso-Gil, U. Stockert, A. P. Mackenzie, D. F. Agterberg, C. Geibel, and E. Hassinger, Field-induced transition within the superconducting state of  $\text{CeRh}_2\text{As}_2$ , *Science* **373**, 1012 (2021).
- [2] K. Semeniuk, M. Pfeiffer, J. F. Landaeta, M. Nicklas, C. Geibel, M. Brando, S. Khim, and E. Hassinger, Exposing the odd-parity superconductivity in  $\text{CeRh}_2\text{As}_2$  with hydrostatic pressure, *Phys. Rev. B* **110**, L100504 (2024).
- [3] J. F. Landaeta, P. Khanenko, D. C. Cavanagh, C. Geibel, S. Khim, S. Mishra, I. Sheikin, P. M. R. Brydon, D. F. Agterberg, M. Brando, and E. Hassinger, Field-angle dependence reveals odd-parity superconductivity in  $\text{CeRh}_2\text{As}_2$ , *Phys. Rev. X* **12**, 031001 (2022).
- [4] Y. Maeno, S. Kittaka, T. Nomura, S. Yonezawa, and K. Ishida, Evaluation of spin-triplet superconductivity in  $\text{Sr}_2\text{RuO}_4$ , *J. Phys. Soc. Jap.* **81**, 011009 (2012).
- [5] K. Nogaki, A. Daido, J. Ishizuka, and Y. Yanase, Topological crystalline superconductivity in locally noncentrosymmetric  $\text{CeRh}_2\text{As}_2$ , *Phys. Rev. Res.* **3**, L032071 (2021).
- [6] T. Yoshida, M. Sigrist, and Y. Yanase, Pair-density wave states through spin-orbit coupling in multilayer superconductors, *Phys. Rev. B* **86**, 134514 (2012).
- [7] D. C. Cavanagh, T. Shishidou, M. Weinert, P. M. R. Brydon, and D. F. Agterberg, Nonsymmorphic symmetry and field-driven odd-parity pairing in  $\text{CeRh}_2\text{As}_2$ , *Phys. Rev. B* **105**, L020505 (2022).
- [8] D. Hafner, P. Khanenko, E.-O. Eljaouhari, R. K uchler, J. Banda, N. Bannor, T. L uhmann, J. F. Landaeta, S. Mishra, I. Sheikin, E. Hassinger, S. Khim, C. Geibel, G. Zwicknagl, and M. Brando, Possible quadrupole density wave in the superconducting Kondo lattice  $\text{CeRh}_2\text{As}_2$ , *Phys. Rev. X* **12**, 011023 (2022).
- [9] S. Ogata, S. Kitagawa, K. Kinjo, K. Ishida, M. Brando, E. Hassinger, C. Geibel, and S. Khim, Appearance of  $c$ -axis magnetic moment in odd-parity antiferromagnetic state in  $\text{CeRh}_2\text{As}_2$  revealed by  $^{75}\text{As}$ -NMR, *Phys. Rev. B* **110**, 214509 (2024).
- [10] S. Ogata, S. Kitagawa, K. Kinjo, K. Ishida, M. Brando, E. Hassinger, C. Geibel, and S. Khim, Parity transition of spin-singlet superconductivity using sublattice degrees of freedom, *Phys. Rev. Lett.* **130**, 166001 (2023).
- [11] K. Nogaki and Y. Yanase, Even-odd parity transition in strongly correlated locally noncentrosymmetric superconductors: Application to  $\text{CeRh}_2\text{As}_2$ , *Phys. Rev. B* **106**, L100504 (2022).
- [12] J. Ishizuka, K. Nogaki, M. Sigrist, and Y. Yanase, Correlation-induced Fermi surface evolution and topological crystalline superconductivity in  $\text{CeRh}_2\text{As}_2$ , *Phys. Rev. B* **110**, L140505 (2024).
- [13] T. Hazra and P. Coleman, Triplet pairing mechanisms from Hund's-Kondo models: Applications to  $\text{UTe}_2$  and  $\text{CeRh}_2\text{As}_2$ , *Phys. Rev. Lett.* **130**, 136002 (2023).
- [14] T. Hotta and K. Ueda, Odd-parity triplet pair induced by Hund's rule coupling, *Phys. Rev. Lett.* **92**, 107007 (2004).
- [15] T. Chen, H. Siddiquee, Q. Xu, Z. Rehfuss, S. Gao, C. Lygouras, J. Drouin, V. Morano, K. E. Avers, C. J. Schmitt, A. Podlesnyak, J. Paglione, S. Ran, Y. Song, and C. Broholm, Quasi-two-dimensional antiferromagnetic spin fluctuations in the spin-triplet superconductor candidate  $\text{CeRh}_2\text{As}_2$ , *Phys. Rev. Lett.* **133**, 266505 (2024).
- [16] S. Khim, O. Stockert, M. Brando, C. Geibel, C. Baines, T. J. Hicken, H. Luetkens, D. Das, T. Shiroka, Z. Guguchia, and R. Scheuermann, Coexistence of local magnetism and superconductivity in the heavy-fermion compound  $\text{CeRh}_2\text{As}_2$  revealed by  $\mu\text{SR}$  studies, *Phys. Rev. B* **111**, 115134 (2025).
- [17] P. Khanenko, J. F. Landaeta, S. Ruet, T. L uhmann, K. Semeniuk, M. Pelly, A. W. Rost, G. Chajewski, D. Kaczorowski, C. Geibel, S. Khim, E. Hassinger, and M. Brando, Phase diagram of  $\text{CeRh}_2\text{As}_2$  for out-of-plane magnetic field, *Phys. Rev. B* **112**, L060501 (2025).
- [18] J. Juraszek, G. Chajewski, D. Kaczorowski, M. Konczykowski, D. F. Agterberg, and T. Cichorek, Nodeless superconducting state in the presence of zero-field staggered magnetization in  $\text{CeRh}_2\text{As}_2$  (2025), [arXiv:2502.14423](https://arxiv.org/abs/2502.14423) [cond-mat.supr-con].
- [19] Y. Wu, Y. Zhang, S. Ju, Y. Hu, Y. Huang, Y. Zhang, H. Zhang, H. Zheng, G. Yang, E.-O. Eljaouhari, B. Song, N. C. Plumb, F. Steglich, M. Shi, G. Zwicknagl, C. Cao, H. Yuan, and Y. Liu, Fermi surface nesting with heavy quasiparticles in the locally noncentrosymmetric superconductor  $\text{CeRh}_2\text{As}_2$ , *Chinese Physics Letters* **41**, 097403 (2024).
- [20] V. G. Yarzhevsky and E. N. Murav'ev, Space group approach to the wavefunction of a Cooper pair, *Journal of Physics: Condensed Matter* **4**, 3525 (1992).
- [21] M. Sigrist and K. Ueda, Phenomenological theory of unconventional superconductivity, *Rev. Mod. Phys.* **63**, 239 (1991).
- [22] T. Micklitz and M. R. Norman, Symmetry-enforced line nodes in unconventional superconductors, *Phys. Rev. Lett.* **118**, 207001 (2017).
- [23] T. Nomoto and H. Ikeda, Symmetry-protected line nodes in non-symmorphic magnetic space groups: Applications to  $\text{UCoGe}$  and  $\text{UPd}_2\text{Al}_3$ , *Journal of the Physical Society of Japan* **86**, 023703 (2017).
- [24] V. G. Yarzhevsky, Space-group approach to the nodal structure of the superconducting order parameter in  $\text{UPt}_3$ , *physica status solidi (b)* **209**, 101 (1998).
- [25] P. W. Anderson, Structure of triplet superconducting energy gaps, *Phys. Rev. B* **30**, 4000 (1984).
- [26] E. A. Teplyakov and V. G. Yarzhevsky, Space-group approach to the Ginzburg-Landau phase winding in topological superconductors: application to  $\text{Sr}_2\text{RuO}_4$ , *Journal of Physics: Condensed Matter* **37**, 185705 (2025).
- [27] V. G. Yarzhevsky and E. A. Teplyakov, Additional quantum numbers for two-electron states in solids. application to topological superconductor  $\text{UPt}_3$ , *Journal of Physics A: Mathematical and Theoretical* **54**, 455304 (2021).
- [28] O. V. Kovalev, *Irreducible Representations of the Crystallographic Space Groups: Irreducible Representations, Induced Representations and Corepresentations* (Gordon and Breach Science, Yverdon, 1993).
- [29] C. J. Bradley and A. P. Cracknell, *The Mathematical Theory of Symmetry in Solids: Representation Theory for Point Groups and Space Groups* (Oxford University Press, Oxford, 1972).

- [30] G. W. Mackey, Symmetric and anti symmetric Kronecker squares and intertwining numbers of induced representations of finite groups, *American Journal of Mathematics* **75**, 387 (1953).
- [31] C. J. Bradley and B. L. Davies, Kronecker products and symmetrized squares of irreducible representations of space groups, *Journal of Mathematical Physics* **11**, 1536 (1970).
- [32] M. Hamermesh, *Group Theory and Its Application to Physical Problems*, Dover Books on Physics (Dover Publications, 2012).
- [33] P. E. Blöchl, Projector augmented-wave method, *Phys. Rev. B* **50**, 17953 (1994).
- [34] G. Kresse and J. Furthmüller, Efficient iterative schemes for ab initio total-energy calculations using a plane-wave basis set, *Phys. Rev. B* **54**, 11169 (1996).
- [35] G. Kresse and D. Joubert, From ultrasoft pseudopotentials to the projector augmented-wave method, *Phys. Rev. B* **59**, 1758 (1999).
- [36] A. V. Krugau, O. A. Vydrov, A. F. Izmaylov, and G. E. Scuseria, Influence of the exchange screening parameter on the performance of screened hybrid functionals, *The Journal of Chemical Physics* **125**, 224106 (2006).
- [37] V. I. Anisimov, J. Zaanen, and O. K. Andersen, Band theory and Mott insulators: Hubbard  $U$  instead of Stoner  $I$ , *Phys. Rev. B* **44**, 943 (1991).
- [38] M. Kawamura, Fermisurfer: Fermi-surface viewer providing multiple representation schemes, *Computer Physics Communications* **239**, 197 (2019).
- [39] J. P. Perdew, A. Ruzsinszky, G. I. Csonka, O. A. Vydrov, G. E. Scuseria, L. A. Constantin, X. Zhou, and K. Burke, Restoring the density-gradient expansion for exchange in solids and surfaces, *Phys. Rev. Lett.* **100**, 136406 (2008).
- [40] A. Ptok, K. J. Kapcia, P. T. Jochym, J. Łażewski, A. M. Oleś, and P. Piekarczyk, Electronic and dynamical properties of CeRh<sub>2</sub>As<sub>2</sub>: Role of Rh<sub>2</sub>As<sub>2</sub> layers and expected orbital order, *Phys. Rev. B* **104**, L041109 (2021).
- [41] X. Chen, L. Wang, J. Ishizuka, R. Zhang, K. Nogaki, Y. Cheng, F. Yang, Z. Chen, F. Zhu, Z. Liu, J. Mei, Y. Yanase, B. Lv, and Y. Huang, Coexistence of near- $E_F$  flat band and van hove singularity in a two-phase superconductor, *Phys. Rev. X* **14**, 021048 (2024).
- [42] S. Ogata, S. Kitagawa, K. Ishida, M. Brando, E. Hassinger, C. Geibel, and S. Khim, Conventional  $s$ -wave superconductivity in LaRh<sub>2</sub>As<sub>2</sub>; the analog without the 4f electrons of CeRh<sub>2</sub>As<sub>2</sub>, *Journal of the Physical Society of Japan* **95**, 013701 (2026).
- [43] V. G. Yarzhevsky, Multiplicity, Parity and Angular Momentum of a Cooper Pair in Unconventional Superconductors of  $D_{4h}$  Symmetry: Sr<sub>2</sub>RuO<sub>4</sub> and Fe-Pnictide Materials, *Symmetry* **13**, 1435 (2021).

## Appendix A: Calculation of two-electron states at symmetry planes, lines and points in a BZ

### 1. Basic equations

One-electron states in a crystal with the symmetry group  $G$  are defined by the wavevector  $k$ , its symmetry group  $H$  (little group) and the index  $\kappa$  of the IR  $D^\kappa$  (small IR) of  $H$  [29]. A left coset decomposition of the

space group  $G$  with respect to its subgroup  $H$  is written as:

$$G = \sum_{\sigma} s_{\sigma} H. \quad (\text{A1})$$

The action of the left coset representatives  $s_{\sigma}$  on the wavevector  $k$  results in a star  $\{k\}$  of this wavevector. An IR of the space group  $G$  is an induced representation  $D^\kappa \uparrow G$  defined by the following formula [29]:

$$(D^\kappa \uparrow G)_{\sigma i \rho j}(g) = \begin{cases} D_{ij}^{\kappa}(s_{\sigma}^{-1} g s_{\rho}), & \text{if } s_{\sigma}^{-1} g s_{\rho} \in H \\ 0, & \text{if } s_{\sigma}^{-1} g s_{\rho} \notin H \end{cases}, \quad (\text{A2})$$

where we use Bradley's notation, with an up arrow for induction [29].

According to the Pauli exclusion principle, the state of two equivalent fermions is antisymmetric with respect to permutation of electrons' coordinates. Hence it follows that the spatial part of a singlet (triplet) pair belongs to a symmetrized (antisymmetrized) direct (Kronecker) square of the IR  $(D^\kappa \uparrow G)(g)$  of the space group. The decomposition of direct squares can be easily done, making use of the Mackey-Bradley theorem on symmetrized squares of induced representations [20, 30, 31] as follows. The space group  $G$  is decomposed into double cosets with respect to the wavevector group:

$$G = \sum_{\delta} H d_{\delta} H \quad (\text{A3})$$

We consider Cooper pairs, i.e., pairs with zero total momentum  $K$ . For any particular space group  $G$  and a wavevector  $k$ , there are different double cosets resulting in the zero total momentum of a pair:

$$K = k + d_{\delta} k = b, \quad (\text{A4})$$

where  $b$  is a reciprocal lattice vector. For generic points inside a BZ,  $d_{\delta}$  is a space inversion, and we have:

$$K = k - k = 0, \quad (\text{A5})$$

On the faces of a BZ there are  $k$  points for which:

$$K = k + k = b, \quad (\text{A6})$$

In this case, the double coset is defined by the identity element  $E$ , and two electrons with the same momenta form a pair. For  $d_{\delta} = E$  and symmorphic groups, symmetrization and antisymmetrization of squares are performed over the group  $H$  according to the standard formula [32]:

$$\chi^{\pm}(D^\kappa \times D^\kappa)(h) = \frac{\chi^2(D^\kappa(h)) \pm \chi(D^\kappa(h^2))}{2}. \quad (\text{A7})$$

In this case spatial parts of both singlet and triplet pairs are even. In non-symmorphic space group for  $k$  at the faces of a BZ IRs  $D^\kappa$  of  $H$  are expressed through projective IRs  $\hat{D}^\kappa$  [28]. The above formula is extended to projective IRs, by taking into account phase factors  $\omega(h, h)$ . Thus, the characters on the wavevector group, corresponding to symmetrized and antisymmetrized squares, respectively, are written as [43]:

$$\chi^\pm(\hat{D}^\kappa \times \hat{D}^\kappa)(h) = \frac{\chi^2(\hat{D}^\kappa(h)) \pm \omega(h, h) \chi(\hat{D}^\kappa(h^2))}{2}, \quad (\text{A8})$$

All possible IRs of the central extension  $\tilde{G}$  corresponding to singlet and triplet pairs are given by inducing these characters into  $\tilde{G}$ .

For each of the self-inverse double cosets, i.e., if:

$$Hd_\alpha H = Hd_\alpha^{-1}H \neq H \quad (\text{A9})$$

we consider an element  $a = dh_1 = h_2d^{-1}$ , where  $h_1, h_2 \in H$ , a subgroup:

$$M_\alpha = aHa^{-1} \cap H \quad (\text{A10})$$

and its extension  $\tilde{M}_\alpha$  by the element  $a$ :

$$\tilde{M}_\alpha = M_\alpha + a M_\alpha, \quad (\text{A11})$$

In the case of a self-inverse double coset, the characters of representations  $P_\alpha^{\kappa\pm}$  of  $\tilde{M}_\alpha$ , correspond to symmetrized and antisymmetrized squares, respectively, and are defined by the following two formulas:

$$\chi(P_\alpha^{\kappa\pm}(m)) = \chi(D^\kappa(m)) \chi(D^\kappa(a^{-1}ma)), \quad m \in M_\alpha \quad (\text{A12})$$

$$\chi(P_\alpha^{\kappa\pm}(am)) = \pm \chi(D^\kappa(amam)), \quad m \in M_\alpha \quad (\text{A13})$$

In the case of Cooper pairs  $d_\alpha = I$ , and  $P_\alpha^{\kappa\pm}$  is a representation of the point group  $\tilde{M}_\alpha$ . Induced representations  $P_\alpha^{\kappa\pm} \uparrow \hat{G}$  give possible symmetries of singlet (triplet) pairs on the whole point group  $\hat{G}$ . This reducible induced representation can be easily decomposed into IRs  $\Gamma^q$  of  $\hat{G}$ , making use of the Frobenius reciprocity theorem, according to which the frequency  $f$  of the appearance of  $\Gamma^q$  in the decomposition of the induced representation is given by the following relation:

$$f(\Gamma^q/P_\alpha^{\kappa\pm} \uparrow \hat{G}) = \frac{1}{|\tilde{M}_\alpha|} \sum_{\tilde{m} \in \tilde{M}_\alpha} \chi^*(\Gamma^q(\tilde{m})) \chi(P_\alpha^{\kappa\pm}(\tilde{m})), \quad (\text{A14})$$

where the vertical bars denote the number of elements in a group.

## 2. Some data about groups $D_{4h}^7$ and $4/mm'm'$

The IRs of the space groups of Kovalev [28] were used in calculations of possible pairs' symmetries, and his digital notations for the group elements  $h_i$  were used in the examples. The correspondence between the digital and standard notation is seen in Table A1, where the elements of the space group  $D_{4h}^7$  are presented. The characters of IRs of the point group  $D_{4h}$  for reflections in planes are presented in Table A2. Negative characters correspond to nodal planes. In the case of zero characters of two-dimensional IRs, the nodes on planes depend on a unitary transformation. Real and complex forms of two-dimensional IRs are presented in Table A3.

The magnetic Shubnikov group with unitary subgroup  $C_{4h}$  may be written as:

$$4/mm'm' = C_{4h} + \vartheta\sigma_y C_{4h} \quad (\text{A15})$$

It is immediately verified that the spatial parts of anti-unitary elements  $B$  are reflections in vertical planes and rotations around horizontal axes by angles  $\pi$ , and hence  $B^2 = E$ . Thus, the sum in Herring's criterion [29] can be easily estimated:

$$\sum_{B \in \vartheta\sigma_y C_{4h}} \chi(B^2) = 8 \quad (\text{A16})$$

Hence, it follows from (A16) that ICRs (irreducible corepresentation) belong to type (a), i.e., they are ordinary IRs for the unitary subgroup  $C_{4h}$  and are extended to the non-unitary left coset with plus or minus sign:

$$\Delta^\pm(R) = D(R), \quad \Delta^\pm(B) = \pm D(BA^{-1})N, \quad N = 1 \quad (\text{A17})$$

ICRs of the group  $4/mm'm'$  are presented in Table A4.

## 3. Symmetry planes in a BZ

On the planes  $k = b_2/2 + \mu b_1 + \nu b_3$  and  $k = \mu b_1 + \nu b_3$  the little group  $H$  consists of the identity element  $E$  and the reflection  $\sigma_y$ . The factor system of the projective representation of the group  $H$  of the wavevector  $k$  is defined as follows:

$$\omega(\alpha, \beta) = \exp(ib \cdot \tau_\beta), \quad (\text{A18})$$

where the reciprocal lattice vector  $b$  is defined by the relation:

$$k - \alpha^{-1}k = b. \quad (\text{A19})$$

It can be seen from (A19) that the first factor in formula (A18) differs from one, if  $\alpha^{-1}$  transforms the wave vector  $k$  into a vector that differs from it by a reciprocal

TABLE A1. Elements of the space group  $D_{4h}^7$  in standard and Kovalev [28] digital notations. Subscripts  $a$  and  $b$  stand for axes (110) and  $(-110)$  respectively, and also for the planes normal to these axes.

	$E, C_{2z}$	$C_{2x}, C_{2y}$	$C_{2b}, C_{2a}$	$C_{4z}, C_{4z}^3$	$I, \sigma_z$	$\sigma_x, \sigma_y$	$\sigma_b, \sigma_a$	$S_{4z}, S_{4z}^3$
Elements	$h_1, h_4$	$h_2, h_3$	$h_{13}, h_{16}$	$h_{14}, h_{15}$	$h_{25}, h_{28}$	$h_{26}, h_{27}$	$h_{37}, h_{40}$	$h_{38}, h_{39}$
$\tau$	(000)	$(\frac{1}{2} \frac{1}{2} 0)$	$(\frac{1}{2} \frac{1}{2} 0)$	(000)	$(\frac{1}{2} \frac{1}{2} 0)$	(000)	(000)	$(\frac{1}{2} \frac{1}{2} 0)$

TABLE A2. Characters of IRs of  $D_{4h}$  for reflections. Negative characters correspond to group theoretical nodal planes obtained by the Mackey-Bradley theorem (see Table I). In the case of zero characters, nodal planes depend on a unitary transformation (see text and Fig. 2).

	$\sigma_x, \sigma_y$	$\sigma_b, \sigma_a$	$\sigma_z$
$A_{1g(u)}$	+1(-1)	+1(-1)	1(-1)
$A_{2g(u)}$	-1(+1)	-1(+1)	1(-1)
$B_{1g(u)}$	+1(-1)	-1(+1)	+1(-1)
$B_{2g(u)}$	-1(+1)	+1(-1)	+1(-1)
$E_{g(u)}$	0	0	-2(+2)

TABLE A3. Matrices of two-dimensional IRs of the  $D_{4h}$  group in real  $E_{g(u)}$  and complex  $\tilde{E}_{g(u)}$  forms. To obtain the matrices on the subgroup  $C_{4v}$  it is sufficient to multiply all matrices for pure rotations by the matrix of the left coset representative  $h_{27} = \sigma_y$ . Two extensions from  $C_4$  to  $C_{4v}$ , differing by the sign of the matrix for  $h_{27}$  are possible. Note that on the subgroup  $C_{4v}$  the matrices of  $\tilde{E}_g$  and  $\tilde{E}_u$  are chosen to be the same. The matrices  $\tilde{E}_g$  and  $\tilde{E}_u$  may be easily extended to  $D_{4h}$  by multiplying them by inversion  $I$  with the signs + or -, respectively.

IR	$h_1$	$h_{14}$	$h_4$	$h_{15}$	$h_{27}$	$h_{27}$
$E_{g(u)}$	$\begin{pmatrix} 1 & 0 \\ 0 & 1 \end{pmatrix}$	$\begin{pmatrix} 0 & -1 \\ 1 & 0 \end{pmatrix}$	$\begin{pmatrix} -1 & 0 \\ 0 & -1 \end{pmatrix}$	$\begin{pmatrix} 0 & 1 \\ -1 & 0 \end{pmatrix}$	$\begin{pmatrix} 0 & 1 \\ 1 & 0 \end{pmatrix}$	$\begin{pmatrix} 0 & -1 \\ -1 & 0 \end{pmatrix}$
$\tilde{E}_{g(u)}$	$\begin{pmatrix} 1 & 0 \\ 0 & 1 \end{pmatrix}$	$\begin{pmatrix} i & 0 \\ 0 & -i \end{pmatrix}$	$\begin{pmatrix} -1 & 0 \\ 0 & -1 \end{pmatrix}$	$\begin{pmatrix} -i & 0 \\ 0 & i \end{pmatrix}$	$\begin{pmatrix} 0 & 1 \\ 1 & 0 \end{pmatrix}$	$\begin{pmatrix} 0 & -1 \\ -1 & 0 \end{pmatrix}$

TABLE A4. ICRs of the magnetic group  $4/m\bar{m}'m'$ , and corresponding angular momentum numbers  $\bar{m}$ .

ICR	$E$	$C_{4z}$	$C_{2z}$	$C_{4z}^3$	$\vartheta\sigma_y$	$\vartheta\sigma_a$	$\vartheta\sigma_x$	$\vartheta\sigma_b$	$\bar{m}$
$A_{g(u)}^+$	1	1	1	1	+1	+1	+1	+1	0, $\pm 4$
$A_{g(u)}^-$	1	1	1	1	-1	-1	-1	-1	0, $\pm 4$
$B_{g(u)}^+$	1	-1	1	-1	+1	-1	+1	-1	$\pm 2$
$B_{g(u)}^-$	1	-1	1	-1	-1	+1	-1	+1	$\pm 2$
$E_{1g(u)}^{'+}$	1	$i$	-1	$-i$	+1	$-i$	-1	$i$	+1
$E_{1g(u)}^{'-}$	1	$i$	-1	$-i$	-1	$i$	+1	$-i$	+1
$E_{2g(u)}^{'+}$	1	$-i$	-1	$i$	+1	$i$	-1	$-i$	-1
$E_{2g(u)}^{'-}$	1	$-i$	-1	$i$	-1	$-i$	+1	$i$	-1

lattice vector  $b$ , and if the improper translation of the second multiplier  $\{\beta|\tau_\beta\}$  has non-zero component in a  $b$  direction.

It can be immediately verified from the data of Table A1, that on all faces of BZ IRs are not projective.

However, the space inversion with an improper translation appears in formula (A12), resulting in a phase factor. Indeed, using multiplication rules for non-symmorphic group elements we obtain:

$$\{I|\tau\}\{\sigma_y|0\}\{I|\tau\} = \{I|\tau\}\{C_{2y}|\sigma_y\tau\} = \{\sigma_y|\tau - \sigma_y\tau\}$$

The translation of the resulting element is written as:

$$\left(\frac{1}{2} \frac{1}{2} 0\right) - \sigma_y\left(\frac{1}{2} \frac{1}{2} 0\right) = \left(\frac{1}{2} \frac{1}{2} 0\right) - \left(\frac{1}{2} - \frac{1}{2} 0\right) = (010)$$

Since the wavevectors on the plane  $k = b_2/2 + \mu b_1 + \nu b_3$  have a constant component  $b_2/2$ , the phase factor -1 appears. In this case, formula (A13) is written as:

$$\{C_{2y}|\tau\}\{C_{2y}|\tau\} = \{E|010\}$$

On the plane  $k = b_2/2 + \mu b_1 + \nu b_3$  this factor also equals to -1. On the plane  $k = \mu b_1 + \nu b_3$  located inside the BZ, additional factors do not arise.

The data for the construction and the results for these planes are presented in Tables A5 and A6. It is seen in these tables, that the non-symmorphic structure of the space group changes the possible pair's symmetry on the lateral faces of the BZ relative to parallel planes passing through the point  $\Gamma$ . In particular, singlet pairs of  $A_{1g}$  symmetry are forbidden on the plane  $k = b_2/2 + \mu b_1 + \nu b_3$ ,

TABLE A5. Construction of Kronecker squares on the plane  $k = b_2/2 + \mu b_1 + \nu b_3$ .

	$E$	$\sigma_y$	$I$	$C_{2y}$	$\text{IR}(\tilde{M})$	$\text{IR}(\hat{G})$
$P^+$	1	-1	1	-1	$B_g$	$A_{2g} + B_{2g} + E_g$
$P^-$	1	-1	-1	1	$A_u$	$A_{1u} + B_{1u} + E_u$

TABLE A6. Construction of Kronecker squares on the plane  $k = \mu b_1 + \nu b_3$ .

	$E$	$\sigma_y$	$I$	$C_{2y}$	$\text{IR}(\tilde{M})$	$\text{IR}(\hat{G})$
$P^+$	1	1	1	1	$A_g$	$A_{1g} + B_{1g} + E_g$
$P^-$	1	1	-1	-1	$A_u$	$A_{2u} + B_{2u} + E_u$

TABLE A7. Construction of Kronecker squares on the planes  $k = \mu b_1 + \nu b_2$  and  $k = b_3/2 + \mu b_1 + \nu b_2$ .

	$E$	$\sigma_z$	$I$	$C_{2z}$	$\text{IR}(\tilde{M})$	$\text{IR}(\hat{G})$
$P^+$	1	1	1	1	$A_g$	$A_{1g} + A_{2g} + B_{1g} + B_{2g}$
$P^-$	1	1	-1	-1	$A_u$	$2E_u$

whereas on the plane  $k = \mu b_1 + \nu b_3$ , singlet pairs of  $A_{1g}$  symmetry are possible. Since the improper translation  $(\frac{1}{2}\frac{1}{2}0)$  has no  $z$  components, the results for planes  $k = \mu b_1 + \nu b_2$  and  $k = b_3/2 + \mu b_1 + \nu b_2$  coincide. These results are presented in Table A7.

#### 4. Symmetry points in a BZ

##### a. Pairing with equal $k$

At points M and A the wavevector group is a  $D_{4h}$  group. Since the improper translation  $(\frac{1}{2}\frac{1}{2}0)$  has no component in  $z$ -direction, the factor systems and the results for these points coincide. In this case wavevector group coincides with the whole group  $G$  and symmetrization is performed by making use of formula (A8). The data for the calculation and the results are presented in Table A8. It is seen in this table, that at points  $M$  and  $A$  singlet pairs (symmetrized squares) may be even and odd, but triplet pairs are odd.

At points X and R space inversion belongs to the wavevector group and two electrons with equal moments form a Cooper pair. In this case symmetrization is performed by making use of formula (A8). The data for calculations and the results for points X and R are presented in Table A9. At these points, singlet pairs may be even or odd, but for triplet pairs only  $E_g$  symmetry is possible.

##### b. Pair density waves at point X

For the double coset, defined by the reflection in a diagonal plane, we have the relation:

$$k_X + \sigma_b k_X = K_M$$

Such two-electron states do not have complete translational symmetry and can be related to pair density waves. The data for the calculation of pair density waves at point X and the results are presented in Table A10. We need to estimate in the product additional phase factors for the elements with non-zero characters of IRs at point X. It so happens that the transformation by element  $h_{37}$  permutes elements  $h_{26}$  and  $h_{27}$ . The characters of the projective representations  $t_{1,2}$  at point X are nonzero only for  $h_{26}$  and equal to zero for  $h_{27}$  (see Table A9), so there is no need to calculate additional factors for the terms  $\hat{D}(d_5^{-1}h_i d_5)\hat{D}(h_i)$ . Going to the squares of left coset element in Mackey-Bradley theorem (see formula (A13)) we ensure that, since  $h_{37}$  and  $h_{40}$  appear without improper translation, the phase factors for the terms  $h_{37}^2$  and  $h_{40}^2$  equal to unity.

Bearing in mind that:

$$h_{13} \cdot \left(\frac{1}{2}\frac{1}{2}0\right) = \left(-\frac{1}{2} - \frac{1}{2}0\right),$$

and that:

$$h_{16} \cdot \left(\frac{1}{2}\frac{1}{2}0\right) = \left(\frac{1}{2}\frac{1}{2}0\right)$$

we can easily estimate the products:

$$\{h_{13}|\frac{1}{2}\frac{1}{2}0\} \cdot \{h_{13}|\frac{1}{2}\frac{1}{2}0\} = \{h_1|000\}$$

$$\{h_{16}|\frac{1}{2}\frac{1}{2}0\} \cdot \{h_{16}|\frac{1}{2}\frac{1}{2}0\} = \{h_1|111\}$$

Hence it follows that the phase factors  $-1$  and  $1$  appear for the terms  $h_{16}^2$  and  $h_{13}^2$  respectively.

These two-electron states at the M have point group symmetry  $D_{4h}$ , but since their total momentum is  $(\frac{b_1}{2}\frac{b_2}{2}0)$ , they are totally symmetric with respect to half of lattice translations only.

TABLE A8. The data for calculations and results (last column) at points M and A

$h$	$h_1$	$h_{14}$	$h_4$	$h_{15}$	$h_2$	$h_{13}$	$h_3$	$h_{16}$	$h_{25}$	$h_{38}$	$h_{28}$	$h_{39}$	$h_{26}$	$h_{37}$	$h_{27}$	$h_{40}$	IR
$h_i^2$	$h_1$	$h_4$	$h_1$	$h_4$	$h_1$	$h_1$	$h_1$	$h_1$	$h_1$	$h_4$	$h_1$	$h_4$	$h_1$	$h_1$	$h_1$	$h_1$	
$\omega_{ii}$	1	1	1	1	-1	1	-1	1	1	-1	1	-1	1	1	1	1	
$t_1$	2	0	-2	0	0	-2	0	2	0	0	0	0	0	0	0	0	
$t_2$	2	0	-2	0	0	2	0	-2	0	0	0	0	0	0	0	0	
$t_3$	2	0	2	0	0	0	0	0	0	0	0	0	0	-2	0	-2	
$t_4$	2	0	2	0	0	0	0	0	0	0	0	0	0	2	0	2	
$\{t_{1,2}^2\}$	3	-1	3	-1	-1	3	-1	3	1	1	1	1	1	1	1	1	$A_{1g} + B_{2g} + B_{2u}$
$\{t_{1,2}^2\}$	1	1	1	1	1	1	1	1	-1	-1	-1	-1	-1	-1	-1	-1	$A_{1u}$
$\{t_{3,4}^2\}$	3	1	3	1	-1	1	-1	1	1	-1	1	-1	1	3	1	3	$A_{1g} + B_{2g} + A_{2u}$
$\{t_{3,4}^2\}$	1	-1	1	-1	1	-1	1	-1	-1	1	-1	1	-1	1	-1	1	$B_{1u}$

TABLE A9. The data for calculation and results (last column) for points X ( $k = \frac{b_2}{2}$  [28]) and R ( $k = \frac{b_2}{2} + \frac{b_3}{2}$  [28]).

IR X, R	$h_1$	$h_3$	$h_2$	$h_4$	$h_{25}$	$h_{27}$	$h_{26}$	$h_{28}$	IR
$t_1$	2	0	0	0	0	0	2	0	
$t_2$	2	0	0	0	0	0	-2	0	
$\omega_{ii}$	1	1	-1	1	-1	1	1	1	
$\{t_{1,2}^2\}$	3	1	-1	1	-1	1	3	1	$A_{1g} + A_{2u} + B_{1g} + B_{2u} + E_u$
$\{t_{1,2}^2\}$	1	-1	1	-1	1	-1	1	-1	$E_g$

TABLE A10. The data for the calculation of pair density waves ( $d_\delta = \sigma_b = h_{37}$ ) at point X.  $K_\delta = K_M$ 

$h_i$	$h_1$	$h_3$	$h_2$	$h_4$	$h_{25}$	$h_{27}$	$h_{26}$	$h_{28}$	formula	IR(M)
$d_\delta^{-1} h_i d_\delta$	$h_1$	$h_2$	$h_3$	$h_4$	$h_{25}$	$h_{26}$	$h_{27}$	$h_{28}$		
$\chi^\pm(h_i)$	4	0	0	0	0	0	0	0	(A12)	
$d_\delta h_i$	$h_{37}$	$h_{38}$	$h_{39}$	$h_{40}$	$h_{13}$	$h_{14}$	$h_{15}$	$h_{16}$		
$d_\delta h_i d_\delta h_i$	$h_1$	$h_4$	$h_4$	$h_1$	$h_1$	$h_4$	$h_4$	$h_1$		
$\chi^+(d_\delta h_i)$	2	0	0	2	2	0	0	-2	(A13)	$t_2 + t_4$
$\chi^-(d_\delta h_i)$	-2	0	0	-2	-2	0	0	2	(A13)	$t_1 + t_3$